Acknowledgements We thank the National Science Foundation, the Petroleum Research Fund administered by the American Chemical Society and the National Institutes of Health for funding, Cambridge Isotope Laboratory for the gift of $^{15}N_2$ and C. A. Bradley for assistance with the indophenolic titrations.

Competing interests statement The authors declare that they have no competing financial interests.

Correspondence and requests for materials should be addressed to P.J.C. (pc92@cornell.edu). X-ray crystallographic coordinates for **1** and **2** have been deposited at the Cambridge Crystallographic Database under numbers 223980 and 223981, respectively.

Low-velocity zone atop the 410-km seismic discontinuity in the northwestern United States

Teh-Ru Alex Song[1], **Don. V. Helmberger**[1] **& Stephen P. Grand**[2]

[1]*Seismological Laboratory, Division of Geological and Planetary Science, California Institute of Technology, California 91125, USA*
[2]*Department of Geological Sciences, UT Austin, Texas 78749, USA*

The seismic discontinuity at 410 km depth in the Earth's mantle is generally attributed to the phase transition of $(Mg,Fe)_2SiO_4$ (refs 1, 2) from the olivine to wadsleyite structure. Variation in the depth of this discontinuity is often taken as a proxy for mantle temperature owing to its response to thermal perturbations. For example, a cold anomaly would elevate the 410-km discontinuity, because of its positive Clapeyron slope, whereas a warm anomaly would depress the discontinuity. But trade-offs between seismic wave-speed heterogeneity and discontinuity topography often inhibit detailed analysis of these discontinuities, and structure often appears very complicated. Here we simultaneously model seismic refracted waves and scattered waves from the 410-km discontinuity in the western United States to constrain structure in the region. We find a low-velocity zone, with a shear-wave velocity drop of 5%, on top of the 410-km discontinuity beneath the northwestern United States, extending from southwestern Oregon to the northern Basin and Range province. This low-velocity zone has a thickness that varies from 20 to 90 km with rapid lateral variations. Its spatial extent coincides with both an anomalous composition of overlying volcanism and seismic 'receiver-function' observations observed above the region. We interpret the low-velocity zone as a compositional anomaly, possibly due to a dense partial-melt layer, which may be linked to prior subduction of the Farallon plate and back-arc extension. The existence of such a layer could be indicative of high water content in the Earth's transition zone.

Spatial variations in topography of the 410-km and the 660-km discontinuities (referred to here as the 410 and 660) are often inferred from SS precursors (length scale of about 1,500–2,000 km)[3,4], near subduction zone depth phase precursors[5], and receiver function analyses (length scale of about 100–300 km)[6–8]. The latest efforts consider simultaneous inverting for both mantle velocity and discontinuity topography[3]. In general, the 660 is depressed under cold regions (slabs) as expected, but the 410 appears to be far more complicated[3–5]. The stacked converted P-to-S phase (Ps) (receiver function) from the 410 is rather weak, complicated and sometimes shows negative pulses above the 410 (ref. 7).

We first compute one-dimensional (1D) full-waveform synthetics[9], model the direct S-wave triplications at epicentral distances of 14–17° and explain the timing and amplitude of multiple arrivals coming from fine structures near the 410 (ref. 10). To resolve the trade-offs between discontinuity topography and mantle velocity directly above or below the discontinuity, we model S-wave triplications at epicentral distances of 21–24°. A low-velocity zone (LVZ) on top of the 410 produces a secondary pulse not normally seen at these distances. Using this secondary pulse as a proxy for the existence of an LVZ atop the 410, we examine events located offshore of Washington–Oregon, USA, and recorded by the TriNet broadband network and several temporary PASSCAL broadband arrays (Fig. 1). Perturbed velocity structures are shown at the turning point for a given great-circle path because the sensitivity to 410 structure is greatest there[11]. The size of the perturbed structure is estimated as the size of the Fresnel zone in both along-path and cross-path directions. We determine a LVZ directly above the 410 in the northwestern US and cross-validate our finding with receiver-function profiles[7].

Record section A shows typical waveform characteristics sampling this area at epicentral distances of 14–17° (Fig. 2a). It samples the region beneath the California-Oregon border (Fig. 1).

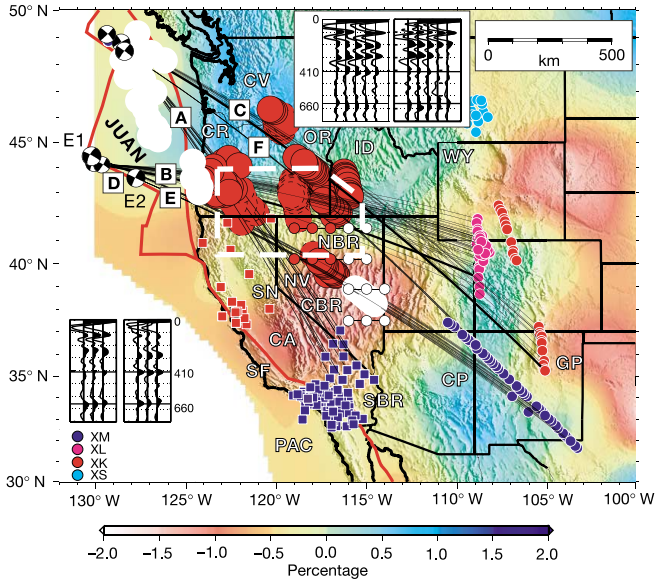

Figure 1 Map of western US displaying samples of fine structure near the 410-km seismic discontinuity. Events off the coast of Oregon and Washington (state borders are in black) are recorded by several PASSCAL arrays (small circles), TriNet (blue squares), and Berkeley network (red squares). Focal mechanisms of these events are shown with black-and-white 'beach balls'. Ray-paths of record sections A–F are shown as black lines. Colour patches display areas sampled by the triplication data; white (normal, no detectable LVZ), large red circles with dashed outline (anomalous 410 with a possible LVZ), large red circles with solid outline (clear LVZ). The areal extent of HAOT[13] is indicated by a heavy white dashed line. The base-colour map shows the variation in SV-shear velocity (relative to the 1D reference model) at a depth of 370 km (ref. 12). Thick red lines show the plate boundary. Top inset, receiver-function determination at 41.5° N, 119°–115° W (left) and 40.2° N, 119°–115° W (right). Bottom inset, receiver-function determination at 38.9° N, 116°–114° W (left) and 37.5° N, 116°–114° W (right). Red dots shown in the map (within Nevada) indicate the location where receiver functions show strong negative pulse above the 410, whereas white dots represent the locations where receiver functions show no negative pulse above the 410 and relatively strong simple 410 peaks. GP, Great Plain; WY, Wyoming; NBR, northern Basin and Range; CBR, central Basin and Range; SBR, south Basin and Range; SN, Sierra Nevada; CV, Cascadia Volcanic Arc; CR, Coast Ranges; JUAN, Juan de Fuca plate; PAC, Pacific plate; SF, San Andreas Fault; CA, California; NV, Nevada; OR, Oregon; ID, Idaho; XM, Rio Grande Rift Seismic Transect array (99/07–01/05); XL, Deep Probe array 97/05–97/11); XK, CDROM (Colorado) array (99/04–00/09); XS, Montana Broadband array (99/11–00/09).

Relative to the 1D reference model (Supplementary Information), we observe a considerable increase of separation in timing between the branch AB and the branch CD of about 4–6 s (Fig. 2a, c). At these ranges, the branch AB represents the S wave propagating through the upper mantle and turning at about 200–300 km, and the branch CD represents the S wave bottoming near the 410 (Fig. 2b). Synthetics calculated from a perturbed 1D model with the 410 depressed by 60 km improve the differential time between the AB and CD branches considerably (model Topo in Fig. 2a). However, other models can also fit the data equally well (Fig. 2a, Supplementary Fig. S1).

Record section B (Supplementary Fig. S2) trends more east–west and samples the region beneath the northern Basin and Range including eastern Oregon, northern Nevada and western Idaho (Fig. 1). This record section shows similar waveforms to those in record section A and previously introduced models can be used to fit the data (Fig. 2c, Supplementary Fig. S2). These record sections indicate that the mantle structure near the 410 is relatively slow beneath the northern Basin and Range. The anomalous structure is probably distributed over areas from the California–Oregon border to the northwestern Basin and Range.

Although it is clear that seismic velocity is slow near 410 km depth, we cannot distinguish between these models: (1) a topographic depression of the 410, (2) a modest decrease in velocity gradient above the 410, (3) a LVZ above the 410, or (4) a hybrid model (LVZA) with the 410 depressed and a LVZ atop the 410 (Fig. 2a, Supplementary Fig. 1). It is difficult to explain this anomaly with current three-dimensional (3D) velocity models[12] because variations in shear-wave velocity at these depths are generally small (Fig. 1).

At the longer epicentral distances of 21–24°, however, it is the branch AB that is bottoming near the 410 (Fig. 2b). In combination with ray-paths at the shorter distances, they provide strong constraints on the structure near the 410. Travel-time curves from model LVZA on top of the 410 not only explain the differential time of branch AB and branch CD at an epicentral distance of 14–17°, but also extend the branch AB from a maximum epicentral distance of 21° to 23° (Fig. 2c).

Record section C (Fig. 3a) samples the northern Basin and Range province and shows an anomalous secondary pulse emerging at epicentral distances of 22–23°, which is also seen in record sections D and F (Fig. 3a, b). The model with a large topographic depression (60 km) of the 410 does not reproduce this feature. The model with a 40-km-thick LVZ containing a 5% reduction in shear velocity produces the observed secondary pulse, but the separation between the first and secondary pulse appears too large (Supplementary Fig. S3). We prefer the hybrid model (LVZA), which explains these record sections in both amplitude and timing. This model has the 410 depressed by 20 km and a 20-km-thick LVZ atop the 410 with a 5% reduction in shear velocity.

Owing to the relatively long period of the S waves (about 6–8 s), a trade-off between the thickness and strength of the LVZ still exists. Therefore, we cannot completely exclude a model having a LVZ of 10 km with 10% velocity drop, or a model having a LVZ of 40 km thick with a 2.5% velocity drop. However, record sections at epicentral distances of 14–17° show that the amplitude of the branch CD predicted by a model having a LVZ with a 10% velocity drop appears too large. Furthermore, receiver-function synthesis (discussed below) indicates that the amplitude of a negative converted pulse due to the existence of a LVZ with only a 2.5% velocity drop cannot explain observed receiver functions. Thus, our preferred model has a 20 km LVZ with a 5% reduction in velocity.

The spatial extent of the LVZ includes regions beneath northern California, Oregon, northern Nevada and southwestern Idaho,

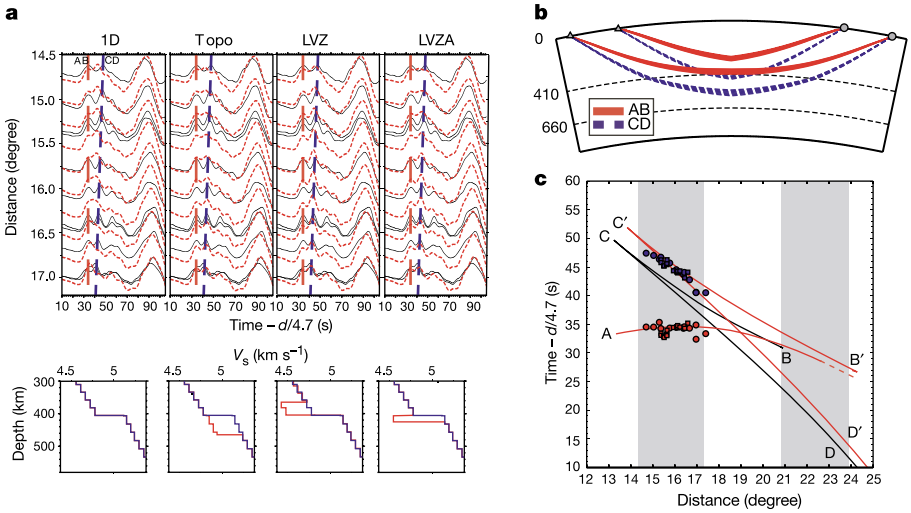

Figure 2 Modelled displacement waveforms (14–17°) with corresponding ray-paths and travel-time triplications. **a**, Record section A (recorded by TriNet, see Fig. 1). Data (solid black traces) are compared with synthetics (dotted red traces) generated from various models, starting from the left: 1D model, model Topo (60 km topography depression), model LVZ (40 km LVZ) and model LVZA (20 km LVZ + 20 km topography depression). Vertical dashed and dash-dotted lines indicate observed triplication branches AB (red) and CD (blue), respectively. Large-amplitude and long-period waves at the end of these traces are Love waves, which are sensitive to the shallow structure. Velocity models used to compute the synthetics are directly shown below these waveforms. The perturbed model is shown as a red line and the reference model is shown as a blue line. The timescale is shown with a reduced velocity of 4.7 km s^{-1}; *d* is epicentral distance. **b**, Ray-paths of triplication branches AB (red line) and CD (blue dashed line). The 410 and 660 seismic discontinuities are given as dashed lines. Note that, at the shorter distance (for example, 16°), the branch CD is primarily sensitive to the structure at the turning point near the depth of 400 km. However, at the longer distance (for example, 22°), the branch AB is primarily sensitive to the same structure. **c**, Triplication curves computed from the 1D model (black line) and model LVZA (thick red line). Observed branches AB and CD of record section A (circle) and record section B (square) are projected with red symbols and blue symbols, respectively (see also Fig. 1 for ray-paths). Note that model LVZA delays the branch CD to fit the above observations but also extends the appearance of the branch AB to epicentral distance of 21–23°.

corresponding to an area of about 100,000 km^2 (Fig. 1). The thickness of the LVZ is about 20 km (Fig. 3a, model LVZA) but appears thicker (70 km thick) beneath the Oregon–Nevada–Idaho border (Fig. 1, Fig. 3a, model LVZB). In central Nevada, the thickness of the LVZ is up to 90 km (Fig. 1, Fig. 3b, model LVZC). However, when examining record section E, we find no evidence for a LVZ atop the 410 beneath the central Basin and Range in eastern Nevada (Fig. 1, Fig. 3b). These observations imply that the variation of the LVZ in thickness is very rapid. This conclusion is supported by receiver function determination[7], where strongly negative pulses directly above the 410-converted pulses suddenly disappear in profiles east of 116° W (Fig. 1). In addition, we note that record sections sampling regions beneath the Juan de Fuca plate show no signs of a LVZ atop the 410 (Fig. 1).

To validate our result, we produce a synthetic receiver function and compare it to the published result[7] for areas closest to that sampled by record section F. The synthetic receiver function from the preferred model LVZB indeed produces a negative pulse associated with the LVZ atop the 410, but the predicted onset of the negative pulse is late and the converted pulse from the 410 is too strong (Fig. 3c). The observed receiver-function determination is constructed through stacking multiple receiver-function profiles from various azimuths where both the thickness of the LVZ and the depth of the 410 are probably changing. Under such circumstances, we can produce the complicated converted pulse from the 410 and the negative pulse from the LVZ on top of the 410 (Fig. 3c, see Supplementary Methods). We could not reproduce receiver functions with a strong negative pulse without inserting a LVZ atop the 410.

We note that strongly negative pulses are absent in areas where we detect no LVZ (Fig. 1, large white circles), whereas converted pulses from the 410 are rather strong and simple (Fig. 1). In general, we expect the amplitude of the converted phase from the 410 to be smaller than that from the 660 because of its smaller velocity contrast. One possible explanation is that these relatively strong converted pulses from the 410 could be related to the existence of a very thin LVZ on top of the 410, which increases the velocity contrast, but if so, it is too thin to be detected.

Geographically, the anomalous region discussed above coincides with a unique type of mantle-derived basalt exposed in the northwestern United States, low-potassium, high-alumina olivine theoleiites (HAOT)[13,14]. Noticeably, HAOT is on average ten times more depleted in incompatible elements than any other type of basalt found in the rest of the Basin and Range and the western USA[13–16]. It is generally believed that formation and eruption of HAOT are strongly linked to extensional tectonics in the back-arc regime. The geographical coincidence between the unique HAOT and the LVZ atop the 410 in the northwestern Basin and Range might suggest that they are probably linked to tectonic processes such as subduction of the Farallon plate and surface extension in the back-arc regime[17]. Other reports of such LVZs directly above the 410 are usually associated with back-arc regimes of ongoing subduction or ancient subduction[5,18–21].

If the LVZ is primarily due to variations in mantle temperature, the thickness of the LVZ is expected to vary gradually. However, the thickness of the LVZ varies rapidly over length scales of about 100–200 km. Therefore, we argue against a thermally dominant origin and prefer a compositional anomaly. The presence of partial melt could considerably lower the velocity[22] but this interpretation is directly linked to the water content actually brought into the deep mantle[23,24]. If the water content is sufficiently high in the transition zone, the LVZ may form directly above the 410 in upwelling material as a result of dehydration melting[25].

For an anhydrous silicate melt, the density of melt can be equal to or larger than that of ambient mantle at depths close to the 410 (refs 26–29). For a hydrous silicate melt, however, not much information is currently available on its density. If the effect of water on the bulk modulus of solids is considered similar to that on the bulk modulus of melts, while the linear relationship between bulk modulus and density holds[30], then hydrous melts may be even denser than hydrous solids. Therefore, the LVZs would be relatively stable for long periods of time. □

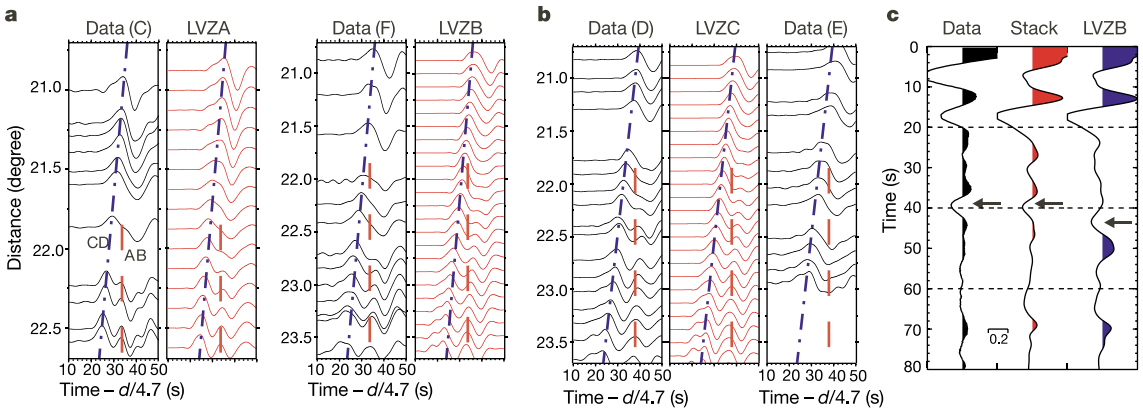

Figure 3 Modelled velocity waveforms (21–24°) and receiver function profiles. **a**, Record section C (recorded by XK PASSCAL stations; see Fig. 1) and synthetics from a hybrid model LVZA (20 km LVZ + 20 km topography depression) are shown in the left two columns. Record section F (recorded by XM PASSCAL stations; see Fig. 1) and synthetics from a hybrid model LVZB (70 km LVZ + 60 km topography depression) are shown in the right two columns. Note that the separation between branches AB and CD is larger in record section F than that in record section C, indicating a thicker LVZ. **b**, Record section D (recorded by XM PASSCAL stations; see Fig. 1) and synthetics from a hybrid model LVZC (90 km LVZ + 60 km topography depression) are shown in the left two columns. Record section E (recorded by XM PASSCAL stations) is shown in the right column. In **a** and **b**, vertical dashed and dash-dotted lines indicate observed triplication branches AB (red) and CD (blue), respectively (see also Fig. 2b). The timescale is shown with a reduced velocity of 4.7 km s^{-1}; *d* is epicentral distance. Triplication branch bottoming beyond the 660 arrives at or even ahead of the CD branch at these ranges. Note record sections D and E sample regions only 100 km apart (see also Fig. 1). No secondary pulse branch AB is observed in record section E at these distances. **c**, Comparison of stacking receiver-function profile[7] and forward calculations. All traces are normalized by the amplitude of the P wave and shown with a ray parameter of 0.06 s km^{-1}. The left trace shows the receiver-function profile, which samples similar regions to record section F (see also Fig. 1). The right trace shows the synthetic receiver function from model LVZB. The middle trace shows a synthetic receiver function by stacking receiver functions computed from multiple 1D models, which have variations in the 410 and the thickness of LVZ (see Supplementary Methods). The arrow points out the negative converted pulse caused by the LVZ on top of the 410.

Received 12 August; accepted 14 November 2003; doi:10.1038/nature02231.

1. Helffrich, G. Topography of the transition zone seismic discontinuity. *Rev. Geophys.* **38,** 141–158 (2000).
2. Shearer, P. M. *et al.* in *Earth's Deep Interior: Mineral Physics and Tomography from the Atomic to the Global Scale* (ed. Karato, S.-I.) 115 (AGU Geophys. Monogr, Vol. 117, Washington DC, 2000).
3. Gu, Y., Dziwonski, A. M. & Ekstrom, G. Simultaneous inversion for mantle velocity and topography of transition zone discontinuities. *Geophys. J. Int.* **154,** 559–583 (2003).
4. Flanagan, M. P. & Shearer, P. M. Global mapping of topography on transition zone velocity discontinuities by stacking SS precursors. *J. Geophys. Res.* **103,** 2673–2692 (1998).
5. Flanagan, M. P. & Shearer, P. M. Topography on the 410 km seismic velocity discontinuity near subduction zones from stacking of sS, sP, and pP precursors. *J. Geophys. Res.* **103,** 21165–21182 (1998).
6. Ramesh, D. S., Kind, R. & Yuan, X. Receiver function analysis of the North America crust and upper mantle. *Geophys. J. Int.* **150,** 91–108 (2002).
7. Gilbert, H. J., Sheehan, A. F., Dueker, K. G. & Molnar, P. Receiver functions in the western United States, with implications for upper mantle structure and dynamics. *J. Geophys. Res.* **109**(B5), doi:10.1029/2001JB001194 (2003).
8. Dueker, K. G. & Sheehan, A. F. Mantle discontinuity structure from midpoint stacks of converted P to S waves across the Yellowstone hotspot track. *J. Geophys. Res.* **102,** 8313–8327 (1997).
9. Saikia, C. K. Modified frequency-wave-number algorithm for regional seismograms using Filons quadrature-modeling of Lg waves in eastern North America. *Geophys. J. Int.* **118,** 142–158 (1994).
10. Grand, S. P. & Helmberger, D. V. Upper mantle shear structure of North America. *Geophys. J. R. Astron. Soc.* **76,** 399–438 (1984).
11. Kennett, B. L. N. & Bowman, J. R. The velocity structure and heterogeneity of the upper mantle. *Phys. Earth Planet. Inter.* **59,** 134–144 (1990).
12. Van der Lee, S. High-resolution estimates of lithospheric thickness from Missouri to Massachusetts, USA. *Earth Planet. Sci. Lett.* **203,** 15–23 (2002).
13. Hart, W. K., Aronson, J. L. & Mertzman, S. A. Areal distribution and age of low-K, high-alumina olivine tholeiite magmatism in the northwestern Great Basin. *Geol. Soc. Am. Bull.* **95,** 186–195 (1984).
14. Hart, W. K. Chemical and isotopic evidence for mixing between depleted and enriched mantle, northwestern USA. *Geochim. Cosmochim. Acta* **49,** 131–144 (1985).
15. Fitton, J. G., James, D. & Leeman, W. P. Basic magmatism associated with late Cenozoic extension in the western United States: Compositional variations in space and time. *J. Geophys. Res.* **96,** 13693–13711 (1991).
16. Kempton, P. D., Fitton, J. G., Hawkesworth, C. J. & Ormerod, D. S. Isotopic and trace element constraints on the composition and evolution of the lithosphere beneath the southwestern United States. *J. Geophys. Res.* **96,** 13713–13735 (1991).
17. Awater, T. & Stock, J. Pacific North America plate tectonics of the Neogene southwestern United States. *Int. Geol. Rev.* **40,** 375–402 (1998).
18. Sacks, I. S. & Snoke, J. A. The use of converted phases to infer the depth of the lithosphere-asthenosphere boundary beneath South America. *J. Geophys. Res.* **82,** 2011–2017 (1977).
19. Revenaugh, J. & Sipkin, S. A. Seismic evidence for silicate melt atop the 410-km mantle discontinuity. *Nature* **369,** 474–476 (1994).
20. Nolet, G. & Zielhuis, A. Low S velocities under the Tornquist-Teisseyre zone: evidence for water injection into the transition zone by subduction. *J. Geophys. Res.* **99,** 15813–15820 (1994).
21. Vinnik, L., Kumar, M. R., Kind, R. & Farra, V. Super-deep low-velocity layer beneath the Arabian plate. *Geophys. Res. Lett.* **30**(1415), doi:10.1029/2002GL016590 (2003).
22. Hammond, W. C. & Humphreys, E. D. Upper mantle seismic wave velocity: Effects of realistic partial melt geometries. *J. Geophys. Res.* **105,** 10975–10986 (2000).
23. Williams, Q. & Hemley, R. J. Hydrogen in the deep Earth. *Annu. Rev. Earth Planet. Sci.* **29,** 365–418 (2001).
24. Dixon, J. E., Leist, L., Langmuir, J. & Schilling, J.-G. Recycled dehydrated lithosphere observed in plume-influenced mid-ocean-ridge basalt. *Nature* **420,** 385–389 (2002).
25. Bercovici, D. & Karato, S. Whole-mantle convection and the transition-zone water-filter. *Nature* **425,** 39–44 (2003).
26. Stolper, E. M., Walker, D., Hager, B. H. & Hays, J. F. Melt segregation from partially molten source regions: the importance of melt density and source region size. *J. Geophys. Res.* **86,** 6261–6271 (1981).
27. Rigden, S. M., Ahrens, T. J. & Stolper, E. M. Densities of liquid silicates at high pressure. *Science* **226,** 1071–1074 (1984).
28. Agee, C. B. Crystal-liquid density inversions in terrestrial and lunar magmas. *Phys. Earth Planet. Inter.* **107,** 63–74 (1998).
29. Chen, G. Q., Ahrens, T. J. & Stolper, E. M. Shock-wave equation of state of molten and solid fayalite. *Phys. Earth Planet. Inter.* **134,** 35–52 (2002).
30. Angel, R. J., Frost, D. J., Ross, N. L. & Hemley, R. Stabilities and equations of state of dense hydrous magnesium silicates. *Phys. Earth Planet. Inter.* **127,** 181–196 (2001).

Supplementary Information accompanies the paper on **www.nature.com/nature**.

Acknowledgements We thank J. Ni, R. Aster, and the rest of the RISTRA team for the use of their data set, and we acknowledge all who have contributed to the PASSCAL arrays and IRIS DMC. We also thank H. Gilbert for providing receiver-function profiles. Reviews from D. Anderson, P. Asimow, T. Ahrens, B. Savage and M. Simons also helped to clarify early versions of this paper. We benefited from discussions with H. Gilbert, D. Anderson, H. Kanamori, Y. Tan, S. Ni and M. Gurnis. We thank L. Zhu for sharing his receiver function modelling code. This study was supported by the NSF and is a contribution to Division of Geological and Planetary Science, Caltech.

Competing interests statement The authors declare that they have no competing financial interests.

Correspondence and requests for materials should be addressed to T.-R.A.S. (alex@gps.caltech.edu).

Mangroves enhance the biomass of coral reef fish communities in the Caribbean

Peter J. Mumby[1], Alasdair J. Edwards[2], J. Ernesto Arias-González[3], Kenyon C. Lindeman[4], Paul G. Blackwell[5], Angela Gall[2], Malgosia I. Gorczynska[2], Alastair R. Harborne[1], Claire L. Pescod[2], Henk Renken[1], Colette C. C. Wabnitz[6] & Ghislane Llewellyn[7]

[1]*Marine Spatial Ecology Laboratory, School of Biological and Chemical Sciences, University of Exeter, Prince of Wales Road, Exeter EX4 4PS, UK*
[2]*School of Biology, Ridley Building, University of Newcastle, Newcastle upon Tyne NE1 7RU, UK*
[3]*Laboratorio Ecología de Ecosistemas de Arrecifes Coralinos, Departamento Recursos del Mar, CINVESTAV Unidad Mérida, AP73 Cordemex, CP97310 Mérida, Yucatán, Mexico*
[4]*Environmental Defense, Caribbean Field Office, Miami, Florida 33186, USA*
[5]*Department of Probability and Statistics, University of Sheffield, Hicks Building, Sheffield S3 7RH, UK*
[6]*Fisheries Centre, Lower Mall Research Station, The University of British Columbia, Vancouver, British Columbia V6T1Z4, Canada*
[7]*Conservation Science Program, WWF-US, 1250 24th Street Northwest, Washington DC 20037, USA*

Mangrove forests are one of the world's most threatened tropical ecosystems with global loss exceeding 35% (ref. 1). Juvenile coral reef fish often inhabit mangroves[2–5], but the importance of these nurseries to reef fish population dynamics has not been quantified. Indeed, mangroves might be expected to have negligible influence on reef fish communities: juvenile fish can inhabit alternative habitats and fish populations may be regulated by other limiting factors such as larval supply or fishing[6]. Here we show that mangroves are unexpectedly important, serving as an intermediate nursery habitat that may increase the survivorship of young fish. Mangroves in the Caribbean strongly influence the community structure of fish on neighbouring coral reefs. In addition, the biomass of several commercially important species is more than doubled when adult habitat is connected to mangroves. The largest herbivorous fish in the Atlantic, *Scarus guacamaia*, has a functional dependency on mangroves and has suffered local extinction after mangrove removal. Current rates of mangrove deforestation are likely to have severe deleterious consequences for the ecosystem function, fisheries productivity and resilience of reefs. Conservation efforts should protect connected corridors of mangroves, seagrass beds and coral reefs.

The Mesoamerican reef system of Belize and Mexico provides a unique experimental setting that has allowed us to isolate the importance of mangroves to coral reef fish. Three atolls have virtually no, or extremely limited, mangrove cover. As migrations from the nearest mangrove resource, across 10–25 km of open ocean with depths exceeding 2,000 m, are likely to be insignificant for demersal reef species[7], we can assume that adult fish must have used nursery habitats, such as seagrass, on the atolls. These reef systems provide three 'scarce mangrove' treatments, in which the mean mangrove perimeter is only 3.9 km within an area the size of Glovers Reef (228 km^2).

Uniquely in the region, Belize also possesses a mangrove-dominated atoll and extensive offshore mangrove islands at the edge of a barrier reef. The offshore barrier reef is separated from the mainland by a channel that is roughly 15-km wide, and sediment cores show that there is little (<1%) connectivity with the mainland[8]. The existence of these offshore, 'rich mangrove' atoll and barrier reef areas allowed us to contrast the fish communities of three mangrove-scarce reef systems with those of three mangrove-rich systems (one atoll and two areas of the barrier reef). The

Supplementary Information

Figure S1 Comparison of displacement data (record section A, black traces) and synthetics (red traces) at epicentral distances of 14-17 degrees.

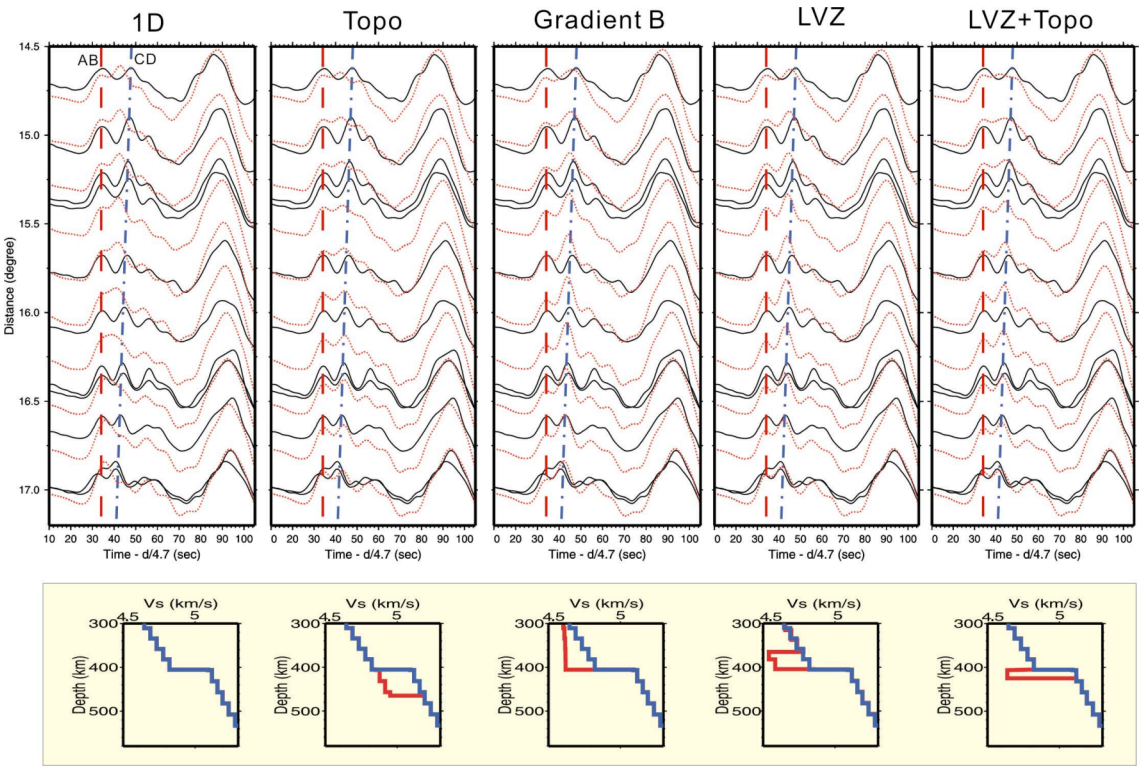

Figure S2 Comparison of tangential displacement data (record section B, black traces) and synthetics (red traces) at epicentral distances of 14-17 degrees.

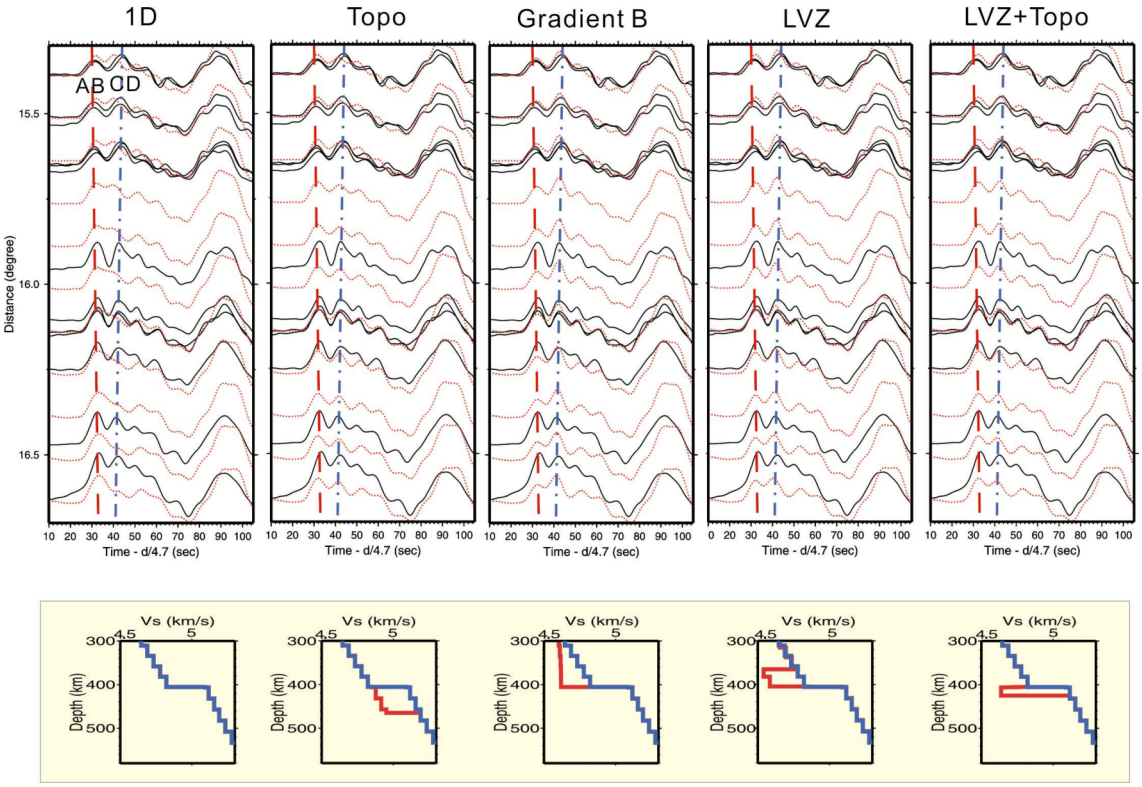

Figure S3 Comparison of synthetics at epicentral distances of 21-23 degrees.

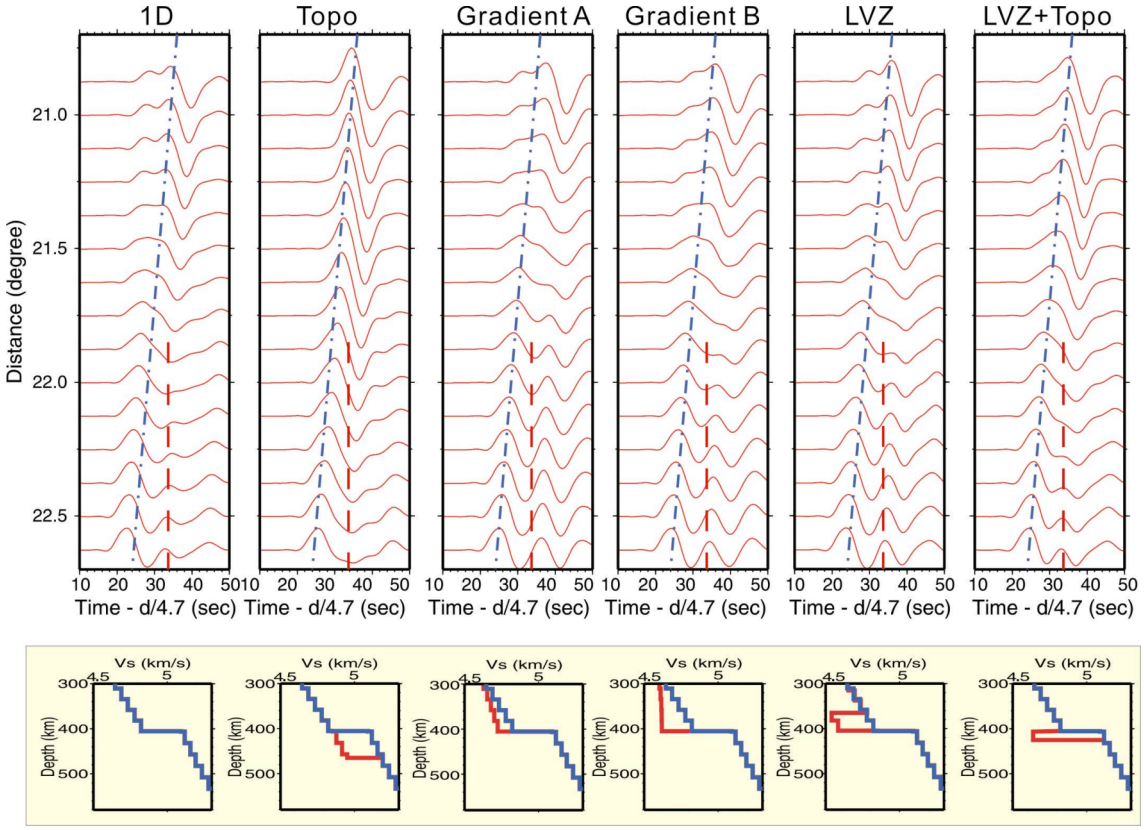

Supplementary Figure Legends

Supplementary Figure 1 Comparison of tangential displacement data (record section A, black traces) and synthetics (red dotted traces) at epicentral distances of 14-17 degrees. Velocity models used in calculating synthetics are shown directly below the record sections. Each inset below the record section shows the perturbed model (red line) and the reference model (blue line). Dashed and dashed-dotted lines indicate triplication branches AB (red) and CD (blue), respectively.

Supplementary Figure 2 Comparison of tangential displacement data (record section B, black traces) and synthetics (red dotted traces) at epicentral distances of 14-17 degrees. Velocity models used in calculating synthetics are shown directly below the record sections. Each inset below the record sections shows the perturbed model (red line) and the reference model (blue line). Dashed and dashed-dotted lines indicate triplication branches AB (red) and CD (blue), respectively.

Supplementary Figure 3 Comparison of synthetics (red traces) at epicentral distances of 21-23 degrees. Synthetics computed from various velocity models, which are shown directly below the synthetics. Each inset below the record sections shows the perturbed model (red line) and the reference model (blue line). Dashed and dashed-dotted lines indicate observed triplication branches AB (red) and CD (blue), respectively. Note models with strong low velocity zone produce the secondary pulse after epicentral distance of about 22 degree.

Supplementary Methods

Waveform modeling

The 1-D reference S model is modified from TNA model[10]. We adopt an average upper mantle velocity from 3-D mantle velocity model constructed for the western United States1[12]. The reference depth of the 410 is at 405 km with 5 % jump in shear velocity. In addition, the thickness of the crust is fixed at 30 km while we vary the thickness of lithosphere (20-40 km) to match the entire waveforms from the AB branch to the Love wave. Synthetics are computed by the FK reflectivity method[9] with earthquake parameters from Harvard Centroid Moment Tensor solutions.

Receiver function modeling

The synthetic receiver function is computed with reflectivity method via a given 1-D velocity model. We simulate stacked receiver function by randomly stacking synthetic receiver functions. Those synthetic receiver functions are computed from velocity models with variations in the thickness (20-90 km) of a LVZ atop the 410 and discontinuity topography (20-60 km). A Gaussian filter of 0.5 Hz is applied to each synthetic receiver function.